Study of L-I-H transition with a new dual gas puff imaging system in EAST superconducting tokamak

G. S. Xu[1],* L. M. Shao[1], S. C. Liu[1], H. Q. Wang[1], B. N. Wan[1], H. Y. Guo[1], P. H. Diamond[2], G. R. Tynan[2], M. Xu[2], S. J. Zweben[3], V. Naulin[4], A. H. Nielsen[4], J. Juul Rasmussen[4], N. Fedorczak[2], P. Manz[2], N. Yan[1,4], R. Chen[1], B. Cao[1], L. Chen[1], L. Wang[1], W. Zhang[1], X. Z. Gong[1]

[1] Institute of Plasma Physics, Chinese Academy of Sciences, Hefei 230031, China
[2] University of California, San Diego, 9500 Gilman Drive, La Jolla, California 92093, USA
[3] Princeton Plasma Physics Laboratory, Princeton, New Jersey 08540, USA
[4] Association Euratom-Risø DTU, DK-4000 Roskilde, Denmark

*E-mail: gsxu@ipp.ac.cn

Abstract: The intermediate oscillatory phase during the L-H transition, termed I-phase, has been studied in the EAST superconducting tokamak by employing a newly developed dual gas puff imaging (GPI) system near the L-H transition power threshold. The experimental observations suggest that the oscillatory behavior appearing at the L-H transition could be induced by the synergistic effect of the two components of the sheared $m,n=0$ **E×B** flow, i.e., the turbulence-driven zonal flow (ZF) and the equilibrium flow (EF). The latter arises from the neoclassical equilibrium, and is, to leading order, balanced by the ion diamagnetic term in the radial force balance equation. A slow increase in the poloidal flow and its shear at the plasma edge are observed tens of milliseconds prior to the I-phase. During the I-phase, the turbulence level decays and recovers periodically. The turbulence recovery appears to originate from the vicinity of the separatrix with clear wave fronts propagating both outward into the far scrape-off layer and inward into the core plasma. The Reynolds work done by the turbulence on the ZFs has been directly measured using the GPI system in the experiments, providing a direct evidence of kinetic energy transfer from turbulence to ZFs, thus driving the ZFs at the plasma edge. The ZFs are damped shortly after turbulence suppression, due to the

loss of turbulent drive, which then leads to the subsequent recovery of the turbulence level, initiating the next dithering cycle, or followed by a final transition into the H-mode, as the EF shear is strong enough to maintain turbulence suppression, even without the assistance of the ZF shear. A new self-consistent zero-dimensional model, incorporating the evolution of the EF and ZF shear, as well as the parallel transport in the scrap-off layer, has been developed and successfully reproduced the L-I-H transition process with many features comparing favorably with the experimental observations.

1. Introduction and brief review of the L-H transition study

One of the most amazing transport phenomena in magnetic fusion plasmas is the spontaneous transition from a low confinement (L-mode) state to a high confinement (H-mode) state with the energy confinement time significantly enhanced, when the input heating power exceeds a threshold level. Elucidating the physical mechanism of the L-H transition is almost 30 years-old endeavor since its first discovery in the ASDEX tokamak [1]. The most important driver for these efforts is the high fusion performance associated with the H-mode due to the formation of a "pedestal" in the pressure profile at the plasma edge, because of the stiffness of the core temperature profiles. Access to H-mode is crucial for the commercial viability of fusion energy. This is particularly critical to ITER, which aims at achieving burning plasmas based on the H-mode confinement. The H-mode operation is also planned even in the initial non-active (non-Deuterium-Tritium) phases in ITER [2]. Given the absence of a reliable predictive model allowing the quantitative evaluation of the L-H transition threshold power in ITER, experimentalists have relied on an international empirical scaling law, which was derived based on the statistical analysis of the experimental database built from the present-day experiments. However, large uncertainties exist in the transition threshold power extrapolated from this scaling law. According to this scaling law, the total input heating power available at the beginning of ITER operation is extremely marginal [3]. Therefore, it may be a big issue for ITER to achieve H-modes in the initial non-active phase with limited power available.

The L-H transition has been the subject of both experimental research in most toroidal

magnetic fusion devices and intensive theoretical and modeling investigations since its discovery [4]. Despite these efforts, the generally weak understanding of turbulence-induced transport in the vicinity of the separatrix between the closed and the open field-line regions prior to the L-H transition has frustrated the search for theory-based models which can account for all experimental observations and give a reliable prediction of the threshold power for H-mode access in ITER. However, substantial evidence has been accumulated over the past two decades that the transport reduction across the L-H transition is due to a sudden suppression of the plasma turbulence level by the $m,n=0$ **E×B** flow shear [5,6], which is generated self-consistently in a narrow layer of the plasma edge with substantially steepened local pressure profile. This leads to the formation of the "edge transport barrier" (ETB), which characterizes the H-mode. Here, n and m are toroidal and poloidal mode numbers, respectively. The shear decorrelation of turbulence has been proposed as a potential mechanism for quenching the turbulence across the transition [7,8], and has been widely supported by experiments [4]. Although significant progress has been made, unfortunately, after two decades of active research the physical mechanism that generates the sheared **E×B** flow and the causality between the flow generation and the L-H transition still remains to be elucidated. In particular, it is unclear whether the enhancement of radial electric field (E_r) and the associated **E×B** flow is a cause or a consequence of the transition since the E_r is strongly coupled with the pressure gradient, which appears to increase more significantly after the L-H transition. Given the unclarified generation mechanisms for the sheared **E×B** flow, it would be very difficult to answer what triggers the L-H transition, or maybe, the L-H transition does not need a trigger at all. The lack of the understanding of these missing pieces has significantly delayed the development of a physics-based model that allows a reliable prediction of the threshold power for H-mode access in ITER. That may also explain why all "first principles" simulation codes have failed miserably at elucidating the L-H transition dynamics, despite multiple attempts have been made [9].

The L-H transition usually occurs very fast with a single sharp reduction of the fluctuation level on the time scale of tens of microseconds when the input heating power is well above the transition threshold or during a fast power ramp-up. However, as the input heating power is close to the transition threshold, an intermediate phase, so called "I-phase", appears prior to

the final transition into the H-mode. This phenomenon was first reported by ASDEX-Upgrade team [10], and was also seen in JET [11], DIII-D [12,13] tokamaks, and W7-AS [4], H-1 [14] stellarators, referred to as “dithering H-mode”, “dithering transition” or recently termed “L-I-H transition”. It appears like a sequence of periodic L-H-L transitions. The number of cycles appearing during the transition increases with a decreasing ramping rate of the input heating power [10]. The repetitive L-H-L transition cycles provide a good opportunity for the study of causality in the transition dynamics. Moreover, near the threshold conditions the transition process becomes much slower with respect to the usual sharp transition, which allows diagnosing the transition process on an expanded time scale.

A predator-prey interaction between edge turbulence and self-generated shear flows during the L-I-H transition was first observed in the H-1 stellarator [14] and later in the DIII-D tokamak [12,13], revealing the critical role of turbulence-driven **E×B** flows in mediating the transition. A model of the L-H transition has been proposed, which successfully reproduced an L-H transition passing through an I-phase, as the transition power threshold is approached [15]. In this model the pre-transition dithering cycles were considered to be a limit-cycle oscillation (LCO) [16], induced by a predator-prey interaction between the edge turbulence and the turbulence-drive “zonal flow” (ZF), and the final transition into the H-mode is due to energy consumption by a second predator - the “mean flow” (MF) or sometimes termed “equilibrium flow” (EF). The ZF and EF are the two components of the total m,n=0 **E×B** flow, with the former being the time-varying component with mesoscale radial structures, driven by the radial gradient of turbulence Reynolds stress [17,18], and the latter arising from the neoclassical equilibrium, largely balanced by the ion diamagnetic term in the radial force balance equation [19,20]. While the EF shear was initially thought to be responsible for the turbulence suppression [5-8], recent studies revealed a critical role of self-generated ZF in regulating turbulence and triggering the transition [18,21]. The model [15] can also reproduce a sharp L-H transition when the input heating power is well above the threshold or ramps up with a much faster rate. For a sharp L-H transition, the multiple transitions during the I-phase are compressed in time into a single-step transition.

Recently, there is renewed interest in the L-H transition physics and power threshold [22-33], stimulated by the ITER requirement for H-mode operation in the initial non-active

phases with limited power available [3], as well as remarkable progress in high-resolution diagnostic capability at the plasma edge that allows us to gain deeper insights into the physics of the L-H transition [34]. Several powerful new diagnostics, such as multichannel Doppler Reflectometry [35-38], gas puff imaging (GPI) [39-41], beam emission spectroscopy (BES) [42,43], and reciprocating Langmuir probes [44-46], have recently been employed in several tokamaks [37-45] and a stellarator [35,36] to study the L-H transition physics near the threshold conditions, with some experimental results comparing favorably with the L-H transition model [15].

More recently, the model has been upgraded from 0D (zero-dimensional) to 1D in space [47], showing that the LCO appears as a nonlinear wave originating from the separatrix and propagating inward. In this model, the transition occurs when the instantaneous ZF shearing rate exceeds the turbulence growth rate, then the energy stored in turbulence is transferred into ZFs and finally dissipated through ZF damping, leading to a net decay of the turbulence energy, thus triggering the L-H transition. During this process, the ZFs play a role of an energy reservoir, mediating the transition by absorbing the free energy of turbulence without increasing turbulent transport. However, since ZFs are turbulence-driven, they can trigger the transition but cannot sustain it. The ZFs will quickly decay when their energy supply - the turbulence - is suppressed. Finally, another player - the EF shear - comes into play, picks up the baton from the ZFs. The transient reduction in turbulence and transport by ZFs allows the edge temperature and density gradients to grow, strengthening the EF shear, which eventually locks in the H-mode state.

Although some debates on the role of ZF as a trigger for the transition still exist, generally speaking, a clearer physical picture of the L-H transition is gradually emerging. An overshoot in the turbulent fluctuation level and ZF amplitude prior to a sharp L-H transition was indeed seen in some experimental cases [48], but not always. One should be aware that the energy transfer from turbulence to large-scale flows is not the only way for turbulence damping. Turbulence level can be suppressed by the well-known shear decorrelation mechanism [7,8], which may directly reduce the effective growth rate of the underlying instability of turbulence. Physically, the shear decorrelation happens because the flow shear increases the effective wave number of the fluctuations [49] in the direction along the shear, i.e., perpendicular to the

flow, which scatters the turbulence spectral power into high-k regions where the dissipation dominates (because the dissipation goes with k^2) [50]. Here k stands for the wavenumber. In experiments, either the L-H transition or the L-I (L-mode to I-phase) transition usually occurs very sharply in time, which may imply some microscopic bifurcation processes from a weak to a strong shear regime behind the L-H transition phenomenon, such as that proposed in a recent work [50].

I-phase has been studied previously in the 2010 experimental campaign on the Experimental Advanced Superconducting Tokamak (EAST), providing the first evidence of the role of ZF for the L-H transition at marginal input heating power [44]. EAST is a fully superconducting tokamak with modern divertor configuration, which commenced operation on September 26, 2006 [51]. To continue our previous work, in the 2012 campaign, a new dual GPI system with two viewing areas separated toroidally and poloidally [52], have been constructed, for the first time, on EAST to provide direct measurements of the spatiotemporal evolution of the turbulence-flow oscillation pattern and turbulence Reynolds stress at the plasma edge near the transition threshold conditions. With this new diagnostic, the time-resolved poloidal and radial plasma flows at two well-separated locations can be obtained simultaneously by tracking the fast motion of turbulence structures in the plane perpendicular to the local magnetic field lines [53], thus allowing the m,n=0 nature, i.e. poloidal and toroidal symmetry, of the zonal flow to be identified, as done previously with other zonal flow diagnostics [21,54,55].

Dedicated experiments have been carried out on EAST in the 2012 campaign to study the transition physics with input heating power close to or slightly above the L-H transition threshold with the newly developed GPI system. Dithering cycles at a frequency from a few hundred Hz to several kHz appeared frequently near the transition threshold conditions. I-phases were observed not only at the L-H transition (L-I-H) but also at the H-L back transition (H-I-L), as well as at the L-to-L transition (L-I-L), i.e., a transition back to L-mode via an I-phase. The L-I-L transitions were only seen when the power was very marginal to the transition threshold, while the L-I-H and H-I-L transitions were sometimes also seen when the power was considerably above, but still within a factor of 2 of the transition threshold. Several L-I-H transitions were captured by the two GPI cameras and reported in this paper.

The experimental observations suggest that the oscillatory behavior appearing at the L-H transition could be induced by the synergistic effect of the EF shear and the ZF shear. Under marginal transition conditions, the evolution of the EF shear is sufficiently slow so that a ZF-driven LCO appears. In the experiments, the turbulence recovery in each dithering cycle was observed to pass through a fast growth phase on a time scale typically less than 100 μs, manifesting itself as an outburst of turbulence across the plasma edge. The turbulent outburst appears to originate from the vicinity of the separatrix with clear wave fronts propagating outward into the far SOL and inward deeply into the plasma. An enhancement in the differential poloidal flows appears periodically at the plasma edge just following the recovery of turbulent fluctuations in each dithering cycle, with a velocity in the electron diamagnetic direction inside the separatrix and in the ion diamagnetic direction outside the separatrix. The turbulence-driven Reynolds work has been directly measured using the GPI system, providing a direct demonstration of kinetic energy transfer from turbulence to ZFs behind the flow generation.

The remainder of this paper is organized as follows. In the following section, a brief introduction of the GPI diagnostic on EAST is given. In section 3, the GPI measurements of an L-I-H transition are described. In section 4, a self-consistent 0D model of the L-I-H transition is described, with comparisons made between modeling and experiments. A summary of the key points is given in section 5, along with conclusions and suggestions for further work.

2. Gas puff imaging system on EAST

The GPI diagnostic is a measuring technique for imaging the local 2D structure and fast motion of the edge plasma turbulence in the plane perpendicular to the local magnetic field lines [56]. A paper with detailed description of the new dual GPI system on EAST has been published recently [52]. Here, only a brief introduction will be given. Figure 1 shows the setup of the new dual GPI system on EAST. It has two imaging objective areas on the low-field side, separated by a toroidal angle of 66.6° and a poloidal angle of roughly 100° around the magnetic axis, with up-down symmetry about the midplane. This special

arrangement allows the direct measurements of plasma perpendicular flows at two well-separated locations on the same magnetic surface, therefore providing a new diagnostic for zonal flows at the plasma edge [21,54,55]. By definition, the zonal flows are uniform flow patterns on the magnetic surfaces with finite radial structures [18,21].

Helium (He) neutral gas was puffed into deuterium plasmas by a gas manifold for each viewing area through 16 holes of 0.5 mm diameter, spaced by 10 mm perpendicular to the local magnetic field. The visible HeI line emission at 587.6 nm from the GPI gas cloud was viewed by two telescopes along the local magnetic field lines to within a few degrees to resolve the radial vs. poloidal structure of the turbulence in a 13 cm by 13 cm square area, as shown in Fig. 1. The blue curve shows the location of the separatrix from the EFIT equilibrium code, which passes through roughly the center of the two viewing areas. The images were recorded simultaneously by two fast cameras at a frame rate of 390804 frames/s and a resolution of 64×64 pixels with 12-bit dynamic range for a capturing time of over 250 ms. The brightness of the HeI during the gas puff is more than ten times higher than the background level before the puff, thus localizing the emission for improved spatial resolution. The spatial resolution of the optical system is ~2 mm at the gas-cloud objective plane, which is smaller than the typical edge turbulence structure size of 10~30 mm measured by reciprocating probes in EAST [57]. The temporal resolution is 2.56 μs and the exposure time is 2.156 μs per frame, which are much shorter than the typical autocorrelation time of the edge turbulence of 10~20 μs [57]. This time resolution is high enough to capture most of the fluctuation spectrum power.

In the collisional radiative approximation and ignoring recombination the intensity of the line emission will depend on the local electron density n_e and temperature T_e as S(photons/m^3) = $n_0 f(n_e,T_e)A$ [56], where n_0 is the local neutral density, A is the radiative decay rate for the observed line, and $f(n_e,T_e)$ is a function that gives the density ratio of neutrals in the upper state to the ground state. The decay rate A, much larger than the inverse of the autocorrelation time of the fluctuations, ensures that the emission corresponds to the local plasma parameters. The functional dependence near the spatial peak of HeI light emission in EAST for typical edge parameters, T_e ~ 30 eV, n_e ~ 5×10^{18} m^{-3}, in this experiment, is $S \propto n_e^{\alpha} T_e^{\beta}$, where typically α, β = 0.5~1 [58,59,41]. Although the exponents vary with n_e and T_e in a complex

way, the local emissivity S is roughly an indicator of the local electron pressure, p_e. Atomic physics calculations indicated that the response time of these lines to changes in n_e or T_e should be ≤ 1μs [41].

For this study, the GPI emission data have been used to obtain the time-resolved poloidal and radial flow velocity, estimated using a time-resolved 2D cross-correlation analysis code based on a modified time-delay estimation (TDE) technique analogous to the one used previously to evaluate poloidal flows from GPI data in NSTX [60,39,40] and C-mod [61,41]. This technique is also similar to the TDE method previously used to evaluate zonal flows from BES turbulence data in DIII-D [62,63]. Although the GPI light emission is a nonlinear function of the local density and temperature, assuming that the neutral density from the gas puff does not vary on the time scale of the turbulence, the turbulence structures and their motion velocities, as determined by the space-time cross-correlation functions of the GPI light fluctuations, are nearly independent of the details of this nonlinearity, as discussed previously [64]. For each GPI viewing area, the local velocities for each pixel have been averaged over the poloidal range of view to evaluate the poloidally averaged large-scale flow component of these velocities.

3. Experimental results from GPI measurements

The new dual GPI system has been employed in a series experiments on EAST in the 2012 campaign to study the L-I-H transition. GPI recordings of three shots, in which the L-I-H transitions were captured in the GPI time sequences, have been analyzed for this study. The phenomena in the three shots are similar, so here only one shot – No. 41363 – will be presented. It is a double-null discharge with major radius R_0 = 1.88 m, minor radius a = 0.45 m, elongation factor κ = 1.7, triangularity δ = 0.47, central-line-averaged density $\bar{n}_e \sim 2.85\times10^{19}m^{-3}$ just prior to the L-I-H transition, toroidal magnetic field B_t = 1.78 T on the magnetic axis, plasma current I_p = 0.4 MA. B_t and I_p are both in the counter clockwise direction viewing from top. Figure 1(a) shows the plasma configuration at the time slice of 3.5 s, along with the two GPI viewing areas and the two midplane reciprocating probes [65].

L-I-H transitions were frequently seen in such plasmas with source power of Low-Hybrid wave Current Drive (LHCD) P_{LHCD} = 1.2 MW at 2.45 GHz, Ion Cyclotron Resonance Frequency (ICRF) heating P_{ICRF} = 1 MW at 27 MHz, and additional 0.1 MW from the Ohmic heating. The total effective heating power is ~1 MW, which is slightly above the transition power threshold under such conditions.

I-phase is characterized by a series of dithering cycles in the D_α emission signals. In shot 41363, a short L-I-L transition with two dithering cycles occurred at 3.518 s, followed by an L-I-H transition with an I-phase from ~3.522 to ~3.530 s, as shown in Fig. 2(a) with the divertor D_α signal measured by a filter scope system focusing on the deuterium α line emission at 656.3 nm. The filter scope system was installed on top of EAST, viewing the lower divertor region through an upper port, with the sightline shown in Fig. 1(a), used to monitor the time evolution of recycling neutrals near the lower divertor targets, which is used as an indicator of the onset of L-H transition and I-phase.

The behavior of dithering cycles in the D_α signal during the L-I-L transition appears to be similar to that during the L-I-H transition. For each dithering cycle, it starts with a peak in the D_α signal, passing through an exponential decay phase typically of ~500 μs, and then followed by a fast growth phase, which is usually within 100 μs. The decay is on the time scale of the SOL particle confinement, $\tau_{||} = L_{||}/(M_{||}C_s)$ ~ 500 μs, where $L_{||}$ (~10 m) is the SOL parallel connection length, $M_{||}$ (~0.4) is the SOL parallel Mach number and $C_s = (2T_e/m_i)^{1/2}$ (~50 km/s) is the sound speed. The growth phase is apparently much shorter than the decay phase, suggesting that each dithering cycle is terminated with an abrupt enhancement in particle transport at the plasma edge. The reduction of D_α light during the quiescent periods is up to 50% in this shot, indicating a significant improvement in particle confinement at the plasma edge. For L-I-L transitions, the D_α level after I-phase is usually higher than or the same as that before I-phase, as seen in Fig. 2(a). However, for L-I-H transitions, the cycle-averaged D_α level in most cases gradually decreases with time, which may suggest a progressive enhancement in particle confinement towards the H-mode.

In addition, it is interesting to notice in Fig. 2(a) that some small-amplitude oscillations at a frequency of several kHz, considerably higher than the repetition frequency of the dithering cycles, appear in the D_α signal preceding the I-phase or between two dithering cycles. The

observation of such oscillations has been reported recently [44] from EAST, showing that small-amplitude oscillations frequently appear hundreds of milliseconds before L-H transitions or after H-L back transitions when the input heating power is marginal to the transition threshold. The small-amplitude oscillations are usually less regular with respect to the normal dithering cycles during I-phase, sometimes even overlapped with some global magneto-hydrodynamics (MHD) perturbations, but exhibit similar features of turbulence-flow interactions at the plasma edge.

Figure 2(b) shows the time history of the radial profile of relative emission intensity from the upper GPI at the plasma edge, displayed in a linear false color scale. The intensity images for each frame has been normalized by the time averaged emission intensity over 2 ms during an L-mode period of 3.520 ~ 3.522 s, in order to eliminate systematic pixel-to-pixel spatial variations due to neutral distribution and optics. The local relative intensity for each pixel has been averaged over the poloidal range of view to remove the poloidal variation. The vertical axis is the distance from separatrix along the minor radius, i.e., $r-r_{sep}$. Positive in the vertical axis corresponds to the region outside the separatrix, i.e. the SOL, with the boundary of the limiter shadow at $r-r_{sep}$ = 3.6 cm. Figure 2(c) shows the poloidally-averaged GPI fluctuation level, which is calculated by applying a high-pass digital filter to remove the fluctuations below 5 kHz, where the dithering cycles and some global perturbations dominate the spectrum.

It is interesting that the GPI emission also shows the dithering cycles nearly in-phase with D_α. Further cross-correlation analysis indicates that the dithering cycles in the GPI emission intensity [Fig. 2(b)] and fluctuation level [Fig. 2(c)] lead the divertor D_α by ~100 μs, which is roughly the SOL parallel communication time with perturbations propagating from the GPI locations to the divertor. When a dithering cycle starts the GPI emission intensity appears to decay outside the separatrix on the same time scale of D_α decay, meanwhile grow inside the separatrix, leading to a substantial increase in the intensity gradient near the separatrix. The increase of emission intensity inside the separatrix could be induced by an accumulation of Helium impurities or an increase in the local electron pressure due to reduced turbulence level and cross-field transport. The intensity changes inside the separatrix as well as in the SOL appear to initiate from the vicinity of the separatrix and expand outward and inward,

respectively, as seen more clearly in the partial enlarged detail in Fig. 3(a).

The difference in the relative GPI emission intensity between two radial locations, i.e., 0.7 cm inside the separatrix and 1.5 cm outside the separatrix, is plotted in Fig. 2(h). The intensity difference grows monotonously during the quiescent period in each dithering cycle, and then suddenly crashes as it reaches a nearly constant threshold level. The flattening of the emission intensity profile is induced by a series of abrupt outbursts of turbulence level at the plasma edge [Fig. 2(c)], which terminate the quiescent periods. The duration of the turbulent outburst is usually ~100 μs, which is much shorter than the quiescent period in each dithering cycle.

The fluctuation level appears to be strongly suppressed during the quiescent periods, which blocks the cross-field transport near the separatrix. The "floodgate" of radial transport, which is closed during the quiescent periods, is then opened by the outburst of turbulence. The accumulated Helium impurities and plasma pressure inside the separatrix during the quiescent period are rapidly released by the strong turbulent ejection, which finally leads to a burst in the divertor D_α recycling signals [Fig. 2(a)] via SOL parallel transport. The turbulent outburst appears to originate from the vicinity of the separatrix with clear wave fronts propagating outward into the far SOL and inward deeply into the plasma (more than 5.5 cm inside the separatrix, limited by the region reachable by the GPI diagnostic) [Fig. 2(b) and (c)]. This observation compares favorably with the recent 1D model, showing that the dithering cycle appears to be a nonlinear wave originating from the separatrix and propagating inward [47].

Space-time patterns of the poloidal motion velocity of turbulence structures from the upper and lower GPI as well as the radial velocity from the upper GPI have been calculated using a modified TDE method and displayed in Figs. 2(d), (e) and (f), respectively. Positive V_r means the velocity outwards along the minor radius. During the turbulent outburst, the turbulence structures inside the separatrix propagate inward, while those outside the separatrix propagate outward at a speed of ~0.2 km/s. The speed is calculated by fitting the slope of the wave-front propagation trajectory, as shown in Fig. 3(b). In addition, the GPI emission intensity in the SOL became progressively lower from one dithering cycle to another [Fig. 2(b)], consistent with the gradually reduced D_α level [Fig. 2(a)]. This may suggest a progressive enhancement in the edge confinement towards the H-mode.

Strong differential poloidal flows appear periodically in a radial range from the SOL up to 2 cm inside the separatrix, accompanying the outbursts of turbulence level. The poloidal velocity is accelerated up to –4 km/s inside the separatrix and 2 km/s in the SOL, where negative velocity corresponds to rotating in the direction of electron diamagnetic drift, i.e., downwards at the outer midplane. The generated flows, especially those in the SOL, appear to delay slightly in time with respect to the outbursts of fluctuation level, as seen in the partial enlarged detail in Fig. 3, which may suggest the causality between them. Correlated poloidal flows observed simultaneously by two GPI cameras at two well-spaced positions on the same magnetic surfaces confirm the ZF characteristics of the flows [21,54,55], thus providing strong evidence for ZF generation during the I-phase.

The Reynolds work performed by the turbulence Reynolds stress on the flows, also known as the energy transfer from turbulence to flows $W_\perp = \partial\left(\left\langle v_r v_p \right\rangle \left\langle v_p \right\rangle\right)/\partial r$ [48,66,67], has been estimated using the time-dependent velocities from the upper GPI and shown in Fig. 2(g), which provides a direct demonstration of nonlinear exchange of energy between turbulence - the prey - and flows - the predator - during the I-phase. Reynolds work gives a measure of the amount of kinetic energy per unit mass and unit time that is transferred between turbulence and flows. Positive $W_\perp$ means net energy transferred from turbulence into flows, so that the flows are amplified at the expense of the turbulence kinetic energy, while negative means energy transfers from flows back into turbulence resulting in flow damping. Therefore, the generation process of flows directly provides a suppression mechanism of turbulence, leading to a net decay of turbulence energy.

Figure 2(g) shows that significant Reynolds work and energy transfer appears only during the turbulent outbursts in a radial region slightly inside the separatrix, i.e., $r-r_{sep} = -2 \sim 0$ cm. The estimated energy transfer rate $W_\perp / v_r^2 \sim 1\times10^6 s^{-1}$ is significantly higher than the typical collisional damping rate of flows ($\sim 2\times10^4 s^{-1}$) or turbulence decorrelation rate ($\sim 1\times10^5 s^{-1}$) at the plasma edge, measured by reciprocating probes in EAST [44,68]. In addition, the energy gain by the flows in one dithering cycle is estimated to be $0.5 m_i V_p^2 \left(1+2q_{95}^2\right) \sim 1\times10^{-18}$ J [44,46], which is of the same order of the energy loss by the turbulence, $e\phi + 0.5 m_i v_r^2$.

Therefore, the energy transfer from turbulence to flows is strong enough to account for the observed flow generation during the I-phase.

Following a turbulent outburst, the turbulence is quickly damped [Figs. 2(c) and 3(b)] as its kinetic energy is released, and possibly its driving force - the pressure gradient - is weakened by the turbulent outburst, which terminates the turbulent state and initiates a quiescent period. Subsequently, the differential poloidal flows decay shortly after turbulence suppression [Fig. 3(c)], due to the loss of turbulent drive. To a certain point, the turbulence level recovers, followed by the initiation of the next dithering cycle.

In addition, it is interesting that some small-amplitude oscillations in D_α, preceding the L-I transitions or between two dithering cycles, act like a transition precursor, and appear to correlate with the oscillations in the turbulence fluctuation level [Fig. 2(c)], the relative GPI emission intensity [Fig. 2(b)] and difference [Fig. 2(h)], as well as the turbulence-driven flows [Figs. 2(d), (e) and (f)]. Although with a smaller amplitude, these oscillations exhibit similar features of turbulence-flow interactions at the plasma edge, e.g., the oscillation (small negative spikes in D_α) at 3.5174 s prior to an L-I transition or at 3.5241 s between two dithering cycles. These small-amplitude oscillations, manifested as small-sized dithering cycles, which have long been ignored previously, could be of high importance for understanding the transition dynamics.

The above observations generally support the theory that turbulence-driven ZFs play a key role in generating the LCOs during the L-H transition [15]. However, the L-H transition cannot be interpreted solely by the ZFs. ZFs could play an important role in mediating the L-H transition but cannot maintain the H-mode state, since the existence of ZFs relies parasitically on the kinetic energy of turbulence. In the absence of a turbulent drive, ZFs will quickly die away. There is another player - the EF shear, which is not driven by turbulence. The EF shear usually builds up as the auxiliary heating power is switched on or ramps up, due to the steepening of edge pressure gradient. It can suppress the edge turbulence due to the well-known shear de-correlation mechanism [5-8], thus push the plasma system towards the transition boundary. During an L-I-H transition, the transient reduction in turbulence and transport by ZF shear during the quiescent periods will allow the edge pressure gradient and therefore the EF shear to increase slowly, which could finally terminate the I-phase and lock

in the H-mode state.

Figures 4(a) and (b) show the time evolution of turbulence poloidal velocity (V_p) and velocity shearing rate ($\partial V_p/\partial r$) across the plasma edge in an expanded time window of the same shot as in Fig. 2. The time windows for the I-phases in Fig. 2 are marked as blue color bars at the top of Fig. 4(a). The auxiliary heating power was switched on at 3.240 s, nearly 290 ms before the H-mode transition at 3.530 s. During this period the plasma density was slowly rising until $\bar{n}_e \sim 2.85\times10^{19}m^{-3}$ just prior to the H-mode transition. As seen in Fig. 4, the poloidal velocity and its shear on both sides of the separatrix slowly increase on a time scale of tens of milliseconds as approaching the final H-mode transition. This slowly evolving poloidal flow is supposed to be associated with the EF. For each time slice in Fig. 4, the velocity is calculated with 800 frames, i.e., time-averaged over ~2 ms, to obtain the velocity profile in the poloidal-radial plane vs. time, then averaged over the poloidal range of view to remove the poloidal variation. However, in H-mode, the turbulence fluctuation level is significantly suppressed so that there is insufficient statistics for the velocity analysis based on the TDE method. As a result, the poloidal velocity and its shear appear to be unreasonably small in the H-mode phase.

Figure 4(c) shows the radial profiles of poloidal velocity, corresponding to three typical time slices marked as vertical lines in Fig. 4(a). The velocity is in the electron diamagnetic direction inside the separatrix and in the ion diamagnetic direction in the SOL, consistent with the observations in many other tokamak experiments [34,67,68]. The poloidal velocity initially exhibits a U-shaped structure of 2 cm in width right inside the separatrix. The bottom of the U-shaped structure evolves slowly with time from −2 km/s in L-mode to −5 km/s in the I-phase just prior to the H-mode transition. In the limiter shadow area, the calculated velocity is in the electron diamagnetic direction, the reason for this is unclear.

No geodesic acoustic mode (GAM) near its characteristic frequency $f_{GAM} = \alpha C_s/R \sim 20$ kHz has been found in either GPI or reciprocating Langmuir probe data near the L-H transitions, where α is a numerical factor depending on the plasma shape. The GAM, frequently observed in L-mode and Ohmic plasmas in EAST, usually disappears as approaching the L-H transition threshold conditions. Similar observations were reported

previously from DIII-D with BES measurements [42,43].

4. Modeling of the L-I-H transition

To facilitate the interpretation of the transition physics, a new self-consistent 0D model, incorporating the time evolution of plasma pressure on both sides of the separatrix, turbulence intensity, EF shear, ZF shear, as well as parallel transport in the SOL, has been developed and successfully reproduces the L-I-H transition process with many features comparing favorably with the above experimental observations. This model consists of four coupled equations:

$$\partial_t p_{edge} = Q - q - q_{neo} \qquad (1)$$

$$\partial_t p_{sep} = q + q_{neo} - p_{sep}/\tau_{\|} \qquad (2)$$

$$\partial_t I = \gamma q I - \alpha V^2 I \qquad (3)$$

$$\partial_t V = \beta I V - \mu(V - U) \qquad (4)$$

Here, Eqs. (1) and (2) describe the time evolution of the pressure inside the separatrix, p_{edge}, and at the separatrix, p_{sep}, respectively. The pressure at the plasma edge, p_{edge}, is enhanced by the power influx from the plasma core, Q, but reduced by the power outflux through turbulent transport, q, and neoclassical transport, q_{neo}, with q presumably much larger than q_{neo} in L-mode but strongly suppressed in H-mode. One new feature distinguishing the model from the previous predator-prey model of the L-H transition [15] is that the SOL physics has been included in Eq. (2). It plays an important role in the transition dynamics, as will be shown later in this article. In the SOL, the imbalance between the power influx through the cross-field transport across the separatrix, $q + q_{neo}$, and the power outflux through parallel transport on a time scale of the parallel communication time, $\tau_{\|}$, drives the time evolution of p_{sep}. Both the turbulent flux and the neoclassical flux are assumed to be driven by the pressure gradient near the separatrix, i.e., $q = \chi I \Delta p$ and $q_{neo} = \chi_{neo} \Delta p$, where $\Delta p = p_{edge} - p_{sep}$ is the pressure difference at the plasma edge, I is the turbulence intensity and χ is the thermal transport coefficient.

The time evolution of the turbulence intensity, I, and the flow shear near the separatrix, $V \propto \partial_r V_{E\times B}$, are controlled by Eqs. (3) and (4), respectively, by extending the previous L-H transition model [15] to combine the contributions from EF shear and ZF shear in one term,

i.e., $\alpha V^2 I$, which represents the Reynolds work done by the turbulence on the flows. The total flow shear, V, is composed of the EF shear, $U \propto \partial_r V_{EF}$, and the ZF shear, $V - U \propto \partial_r V_{ZF}$, where $V_{EF} + V_{ZF} = V_{E\times B}$. Here, all turbulence-driven flows are classified as ZFs. The above set of equations is closed by the following expression of EF shear, $U = \kappa \Delta p$. The EF arises from the neoclassical equilibrium, to leading order, balanced by the ion diamagnetic term in the radial force balance equation, therefore proportional to the pressure gradient.

The free energy stored in the pressure gradient is released and part of this is deposited in the turbulence through Eq. (3). The turbulence in this model is assumed to be flux driven and suppressed by the flow shear due to transfer of kinetic energy from the turbulence into the sheared flows via the Reynolds work, so that the first term on the right-hand side of Eq. (3) is proportional to q and the second term is proportional to V^2. The transferred energy then drives the sheared flows through the first term on the right-hand side of Eq. (4), following the expression in the reference [15]. Finally, the energy is released through dissipation, as described by the last term in Eq. (4), where the sheared flows are subjected to strong frictional damping. Here, μ is the total flow damping rate, including damping effects from collision, charge exchange, neutral friction, and other nonlinear mechanisms. According to Eq. (4), in the absence of turbulence ($I \to 0$), such as in the case of H-mode, the flow shear, V, will relax towards the EF shear, U, since in the absence of turbulent drive, the ZF shear, $(V - U)$, is going to vanish.

This system of equations has been solved numerically based on an explicit 4-order Runge-Kutta method, starting from an L-mode stationary state, evolving across an I-phase and ending with a quiescent H-mode. Figure 5 shows the modeling results, including the time evolution of pressure at the separatrix (p_{sep}) and inside the separatrix (p_{edge}), edge pressure difference (Δp), turbulence intensity (I), total flow shear (V), EF shear (U), turbulent flux (q), neoclassical flux (q_{neo}), imbalance between the drive and damping of turbulence on the right-hand side of Eq. (3), and input heating power flux (Q), assuming constant values for the other coefficients. The external control parameter of the system is Q, which is the source of free energy. It increases from unity at a slow ramping rate of $10^{-4}\times$time, as shown in Fig. 5(g).

This system of equations has two stationary solutions. One is the H-mode, for which the turbulence intensity and the turbulent flux vanish. Without the turbulent transport, the input

heating power can only be carried out through the neoclassical flux, $q_{neo} = Q$, so that the edge pressure gradient is determined solely by the neoclassical transport, $\Delta p = Q/\chi_{neo}$. In the SOL the neoclassical flux is balanced by the parallel flux, which makes the SOL pressure dependent on Q, i.e., $p_{sep} = \tau_{\|}Q$. The pressure inside the separatrix is therefore proportional to Q with $p_{edge} = Q/\chi_{neo} + \tau_{\|}Q$. In addition, the flow shear is clamped to the EF shear, i.e., V = U, which is also an increasing function of Q.

The other stationary solution is the L-mode, which is characterized by a finite level of turbulence and turbulent flux. A set of initial values, which satisfies the set of equations for an L-mode stationary state, has been applied to the L-I-H transition model, as listed in Table 1.

Table 1. A set of initial values for the L-mode stationary solution of the L-I-H transition model

Q	p_{edge}	p_{sep}	Δp	I	V	U	q	q_{neo}	$\tau_{\|}$	γ	α	β	μ	χ	χ_{neo}	κ
1	20	10	10	2	0.5	0.1	0.9	0.1	10	1	3.6	1	2.5	0.045	0.01	0.01

The evolution of the system starts from an L-mode stationary state defined by the above set of initial values. As the input heating power, Q, slowly ramps up linearly, the system passes through three distinct phases, as indicated in Fig. 5. The early phase is an L-mode, during which small-amplitude oscillation appears and grows into normal dithering cycles after several oscillation periods. Such small-amplitude oscillations prior to I-phase or L-H transition has been observed in experiments, as shown in Fig. 2(a), described in section 3.

The L-mode phase is followed by an I-phase, characterized by dithering cycles. The time waveform of p_{sep} [Fig. 5(a)] resembles the D_α waveforms very much, since the pressure drives the SOL parallel flows and therefore the divertor D_α emission from the recycling neutrals. It is interesting to notice in Fig. 5 that the cycle period increases with time as approaching the final H-mode transition. This phenomenon has been frequently seen in our experiments, which could be due to progressive enhancement of the EF shear during the I-phase.

The I-phase is finally terminated by a transition into the H-mode phase, with significantly suppressed turbulence and turbulent flux [Figs. 5(c) and (e)], leading to a fast growth of the pressure inside the separatrix and the edge pressure gradient [Fig. 5(b)]. The

neoclassical transport then takes over from the turbulent transport with the flow shear, V, tracking the EF shear, U, closely [Fig. 5(d)]. The final transition from I-phase to H-mode occurs when a threshold level in the EF shear, U, is crossed, followed by a progressive enhancement in the edge pressure gradient, Δp, during the I-phase.

According to Eq. (2), the decay of p_{sep} and therefore the D_α emission across the H-mode transition or during the decay phase of each dithering cycle is on the time scale of the SOL parallel loss, $\tau_{\|}$, consistent with experiments. Furthermore, the time scale for the growth phase of p_{sep} during one dithering cycle, i.e. that for replenishing the SOL by the turbulent outburst, is apparently much shorter than the decay phase, and the cycle-averaged p_{sep} appears to decrease progressively during the I-phase as approaching the final H-mode transition. All these features compare favorably with experiments, as shown in Fig. 2(a), described in section 3. In addition, the slow rising of the pressure inside the separatrix and the edge pressure gradient during the I-phase [Fig. 5(b)], together with the gradual reduction in the cycle-averaged p_{sep}, may suggest a progressive enhancement in the edge confinement towards the H-mode.

With the help of the model, we are allowed to have a deeper insight into the physics behind the L-H transition. The ZFs have been proposed as a candidate for triggering the transition in the popular theory [15]. The energy transfer from turbulence to ZFs can lead to the suppression of turbulence level as well as ZF generation. In the L-mode stationary state, it has been shown in experiments that finite energy transfer from turbulence to ZFs exists at the plasma edge, which maintains a saturated level of low frequency ZFs [21,45,54,55,67]. At the transition to the H-mode or in the quiescent period of a dithering cycle, a mechanism is required to initiate a fast energy transfer process or other turbulence damping processes, so that the edge turbulence can be quenched in a short period. However, since the ZF is turbulence driven, it cannot suppress the turbulence alone without a pronounced overshoot in the ZF amplitude or a sharp increase in the energy transfer rate from turbulence to ZFs. If there is an overshoot in the ZF amplitude, an outburst of turbulence is required prior to the overshoot to drive the ZFs so that they have sufficient amplitude to quench the turbulence. The puzzle is not regarding the causality between turbulence suppression and ZF generation, since they occur simultaneously during the energy transfer process, but regarding what

initiates the fast energy transfer process across the transition.

This puzzle can be solved when another player is taken into account, i.e., the EF shear. The successful reproduction of an L-I-H transition by the above modeling suggests that the transition and the oscillatory behavior during an I-phase could be induced by the synergistic effect of the ZF and the EF, instead of solely by the action of ZF. As indicated by the model, two feedback loops exist at the plasma edge, associated with the two flow components, i.e., the ZF and the EF, respectively, through which the fast energy transfer process and turbulence suppression at the transition are initiated.

Figure 6 shows a schematic block diagram of the two feedback loops in the model. The oscillatory behavior and fast energy transfer at the transition are controlled by a fast feedback loop associated with the ZF shear, $(V - U)$, which cannot be activated by itself when the system is far below the transition threshold. It needs another feedback loop, i.e., that associated with the EF shear, to push the system towards the transition boundary. The latter is a positive feedback loop, evolving on the time scale of local transport, which is much slower compared to the dithering cycle period.

As approaching the transition threshold, heat and particles accumulate at the plasma edge with increasing heating power, Q, resulting in an increase of the pressure inside the separatrix, $\langle p_{edge} \rangle$, which drives the EF shear, $\langle U \rangle$, where $\langle \cdots \rangle$ denotes the time average over a dithering cycle period. The EF shear promotes the energy transfer from turbulence to ZFs through the Reynolds work. When the energy loss of the turbulence exceeds the energy gain, i.e., $\gamma q < \alpha V^2$, the turbulence starts to be suppressed, which initiates the dithering cycles in the fast feedback loop. On the other hand, the cycle-averaged turbulent flux, $\langle q \rangle$, is reduced, which then further enhances the pressure inside the separatrix, $\langle p_{edge} \rangle$, enabling the system to evolve towards the H-mode. This positive feedback loop controls the transition direction. This evolution direction can be reversed if the power flux, Q, ramps down instead of ramping up. Any perturbation in Q, such as the transiently enhancement in power flux by a sawtooth heat pulse [69], can accelerate or slowdown the positive feedback, and therefore promote or delay the transition process.

For the fast feedback loop, dithering cycles are activated only when the transition power threshold is approached. The oscillation can be amplified, as seen in Fig. 6, since free energy

stored in the pressure gradient can be fed into the turbulence-ZF system through the turbulence drive. In our experiments, dithering cycles with increasing oscillation amplitudes towards the final H-mode transition are frequently observed.

A dithering cycle starts with turbulence suppression, I↓, which initiates a quiescent period. Heat and particles are accumulated inside the separatrix, enhancing the edge pressure, p_{edge}↑, as the cross-field transport at the plasma edge is suppressed. In the SOL, since the particle and heat source are reduced, the pressure decays, p_{sep}↓, on the time scale of the SOL parallel loss, $\tau_{||}$, together with the enhanced p_{edge}, leading to an increase in the pressure gradient near the separatrix, Δp↑, which then enhances the turbulence drive. On the other hand, with reduced ZF drive, the flow shear, V, relaxes towards the EF shear, U, i.e., the ZF shear is damped subsequently, $(V - U)$↓, which then reduces the damping of turbulence. To a certain point, the combined effects make the turbulence drive exceed the turbulence damping, i.e., $\gamma q > \alpha V^2$ [Fig. 5(f)], so that the turbulence starts to grow in intensity, i.e., I↑. This growth eventually evolves into an outburst of turbulence as shown in Fig. 5(c).

The "floodgate" of the cross-field transport, which is blocked during the quiescent period, is then opened by the outburst of turbulence [Fig. 5(e)]. The accumulated pressure inside the separatrix, p_{edge}, during the quiescent period is rapidly released by the strong turbulent ejection, which flattens the pressure profile near the separatrix [Fig. 5(b)], and replenishes the SOL with fresh particles and heat, leading to a quick recovery of the pressure at the separatrix, p_{sep} [Fig. 5(a)]. At the same time, pronounced ZF shear, $(V - U)$↑, is driven by the turbulent outburst [Fig. 5(d)], which significantly enhances the damping of turbulence. Meanwhile, the turbulence drive is weakened due to the reduced pressure gradient, Δp↓, so that the turbulence damping exceeds the turbulence drive very quickly, i.e., $\gamma q < \alpha V^2$ [Fig. 5(f)], leading to a sharp decay in the turbulence intensity [Fig. 5(c)] and the turbulent flux [Fig. 5(e)]. During this process, the free energy stored in turbulence is transferred into the ZFs via the Reynolds work, driving the ZF shear, and finally released through ZF damping. When the turbulence is suppressed, i.e., I↓, the system evolves into a quiescent period again. Then, a new dithering cycle starts.

Finally, the I-phase is terminated by a sharp transition into the H-mode, as the EF shear, U, is strong enough to take over from the ZF shear, stopping the recovery of the turbulence

intensity, and thus locking in the H-mode state. By comparing with the experimental results shown in Fig. 2, one can see that many features from the modeling are in good agreement with the experimental observations.

In addition to the L-I-H transition, the model successfully reproduces a sharp L-H transition, i.e., an L-H transition without passing through an I-phase. The L-I-H transition shown in Fig. 5 is obtained with a slow ramping rate of the heating power flux, Q. With a faster ramping rate, fewer dithering cycles appear. Furthermore, as the ratio of initial value U to V increases to a certain level, the I-phase is compressed into a single sharp L-H transition, since the EF shear increases so quickly that it dominates over the contribution from the ZF shear in the Reynolds work term, $\alpha V^2 I$, which results in a net decay of the turbulence energy due to energy transfer into ZFs till the H-mode state is reached. In the H-mode, although the driving forces of turbulence - the pressure gradient - increases, the damping by the EF shear is so strong that it stops the recovery of the turbulence level.

In addition, the model has been used to study H-L back transition. I-phases during the H-L back transition similar to that appearing during the L-H forward transition as well as the so-called “hysteresis effect” in the transition power threshold have also been successfully reproduced by this model. However, it is beyond the scope of this article, and will be discussed in future publications.

5. Summary and discussions

In summary, dedicated experiments have been carried out on EAST in the 2012 campaign with a newly developed dual GPI system [52,53] to study the L-I-H transition with input heating power close to or slightly above the L-H transition threshold. With the new dual GPI system, the time-resolved poloidal and radial plasma flows as well as the turbulence-driven Reynolds work at two well-separated locations can be obtained simultaneously by tracking the fast motion of turbulence structures in the plane perpendicular to the local magnetic field lines. It provides a new diagnostic for zonal flows at the plasma edge [21,54,55], thus allowing us to gain a deeper insight into the details of the transition dynamics. To facilitate the interpretation of experimental data, a new self-consistent 0D model,

incorporating the time evolution of plasma pressure on both sides of the separatrix, turbulence intensity, EF shear, ZF shear, as well as parallel transport in the SOL, has been developed and successfully reproduced the L-I-H transition process with many features comparing favorably with the experimental observations. In addition, the background and the state of the art of this research topic have been reviewed briefly in this article.

A couple of interesting features of the L-I-H transition have been observed, for the first time, with the new dual GPI diagnostic:

- A slow increase in the poloidal flow and its shear at the plasma edge are observed tens of milliseconds prior to the I-phase. This slowly evolving poloidal flow is supposed to be associated with the EF.
- The fluctuation level appears to be strongly suppressed during the quiescent period in each dithering cycle. With reduced cross-field transport, the GPI emission intensity grows inside the separatrix and decays in the SOL, leading to a monotonous increase in the gradient near the separatrix. The gradient then suddenly crashes as it reaches a nearly constant threshold level, terminating the quiescent period.
- The flattening of the emission intensity profile is induced by a series of abrupt outbursts of turbulence at the plasma edge, with a fast growth phase typically less than 100 μs, which is much shorter than the quiescent period, typically of ~500 μs, in each dithering cycle.
- The turbulent outburst appears to originate from the vicinity of the separatrix with clear wave fronts propagating both outward into the far SOL and inward deeply into the plasma at a speed of ~0.2 km/s along the minor radius. This observation compares favorably with the recent 1D model, showing that the dithering cycle appears to be a nonlinear wave originating from the separatrix and propagating inward [47].
- An enhancement in the differential poloidal flows appears periodically in a radial range from the SOL up to 2 cm inside the separatrix just following the recovery of turbulent fluctuations in each dithering cycle, with a velocity up to –4 km/s in the electron diamagnetic direction inside the separatrix and up to 2 km/s in the ion diamagnetic direction outside the separatrix.
- The Reynolds work done by turbulence on ZFs has been directly measured with the GPI

system in the experiments, showing a significant magnitude during the turbulent outbursts in a radial region slightly inside the separatrix, i.e., $r-r_{sep} = -2 \sim 0$ cm, which provides a direct evidence of kinetic energy transfer from turbulence to ZFs, thus driving the ZFs at the plasma edge.

- Following a turbulent outburst, the turbulence is quickly damped as its kinetic energy is released, and possibly its driving force - the pressure gradient - is weakened by the turbulent outburst, which then terminates the turbulent state and initiates a quiescent period. Subsequently, the differential poloidal flows decay shortly after turbulence suppression, due to the loss of turbulent drive. To a certain point, the turbulence level recovers, then initiating the next dithering cycle.
- Some small-amplitude oscillations in D_α emissions, appearing to be small-sized dithering cycles, at a frequency of several kHz, considerably higher than the repetition frequency of the normal dithering cycles, are frequently present prior to the I-phase or the L-H transition, acting like a transition precursor. Although with a smaller amplitude, these oscillations exhibit similar features of turbulence-flow interactions at the plasma edge.
- No GAM oscillation near its characteristic frequency has been found in either GPI or reciprocating Langmuir probe data near the transition threshold conditions or in H-mode.

The experimental results as well as the successful reproduction of the L-I-H transition by the 0D model suggest that the transition and the oscillatory behavior during the I-phase could be induced by the synergistic effect of the two components of the sheared m,n=0 **E×B** flow, i.e., the ZF and the EF. The total **E×B** flow is the leading order perpendicular guiding-center flow [70], which can be decomposed into two components according to their generation mechanisms [5]. One is the EF, which is a natural product of the neoclassical equilibrium, to leading order balanced by the ion diamagnetic term ($\partial_r p_i / Z_i e n_i B^2$) in the radial force balance equation [19,20]. The other is the ZF, which is driven by the plasma turbulence through the turbulence Reynolds work [17,18]. As indicated by the model, two feedback loops exist at the plasma edge, associated with the two flow components, through which the fast energy transfer process and turbulence suppression at the transition are initiated. The experimental and

modeling results presented in this article strongly suggest the following physical picture of the L-I-H transition:

Turbulence suppression at the L-H transition could be induced by a reduction in turbulence energy input or by an enhancement in turbulence energy output. The turbulence energy input can be reduced due to the shear decorrelation mechanism through the reduction of the effective growth rate of the underlying instability of turbulence [5-8]. For the turbulence energy output, one important channel is transferring the kinetic energy downward in the frequency domain from turbulence to low frequency ZFs [17,18]. Another channel is scattering the turbulence spectral energy into the high-k dissipation regions [50]. Both the shear decorrelation and the energy transfer or scattering are controlled by the total m,n=0 **E×B** flow shear due to tilting and breaking of turbulence eddies [5-8]. For each limit cycle oscillation, the cycle starts with the suppression of the turbulence by the total **E×B** flow shear, leading to the subsequent damping of the ZFs, due to the loss of turbulent drive. To a certain point, the total **E×B** flow shear is insufficient to maintain turbulence suppression, so that the turbulence level recovers, which initiates the next dithering cycle. In addition, during the I-phase, the turbulence is periodically suppressed across the sheared region of the plasma edge, thus allowing the local pressure gradient and consequently the EF shear to build up progressively, which finally locks in the H-mode state.

In addition, our experiments suggest that the SOL physics could also play a role in the transition dynamics. The SOL parameters set the boundary conditions for the dynamics inside the separatrix. For instance, a reduction in the SOL pressure will contribute to an enhancement in the pressure gradient near the separatrix. This pressure gradient controls the EF, which has been shown to play an important role in the transition physics. An exponential decay in the divertor D_α emission as well as the GPI emission intensity in the SOL has been observed during the quiescent period in each dithering cycle, on a time scale of the SOL particle confinement, $\tau_{||} = L_{||}/(M_{||}C_s) \sim 500$ μs. During the quiescent period, the particle and heat sources in the SOL are significantly reduced, since the cross-field transport is blocked by the flow shear at the plasma edge. The particle and heat in the SOL are therefore gradually exhausted through parallel transport, resulting in the exponential decay. When a turbulent outburst occurs, the accumulated pressure inside the separatrix during the quiescent period is

rapidly released by the strong turbulent ejection, which replenishes the SOL with fresh particles and heat, leading to a quick recovery of the SOL pressure.

Some critical issues still need to be addressed in future work:

- Is a "trigger" necessary for the transition? What is the dominant reason for the turbulence suppression during the transition - reduction in turbulence energy input or enhancement in turbulence energy output? One should be aware that the energy transfer from turbulence to large-scale flows is not the only way for turbulence damping. There are other channels for turbulence damping. For instance, it is well known that turbulence can be suppressed by the flow shear due to scattering the turbulence spectral energy into high-k regions where the energy is dissipated [50]. In addition, we still cannot rule out the possibility of some microscopic bifurcation processes from a weak to a strong shear regime sitting behind the L-H transition phenomenon, such as that proposed in a recent work [50].
- How to bridge the microscopic to the macroscopic? How do the transition dynamics enter the transition power threshold scaling? What is the microscopic mechanism behind the "density roll over"?
- Does the H-L back transition retrace the route of forward transition, i.e. revisits I-phase? Are the small type-III-like ELMs during the H-L back transition really LCOs? What is the microscopic physics of the "hysteresis"?
- Does the toroidal rotation and momentum transport play a role in the transition? The toroidal rotation was thought to be subject to strong charge exchange damping at the plasma edge, therefore ignored in the previous 1D transition model [47]. However, the damping could be weak in the low-collisionality edge plasmas of the future fusion reactors.
- How does the recycling and neutral physics influence the power threshold, apart from charge exchange damping? Experiments show strong dependence of the transition power threshold on the wall conditions and impurity concentration [33], however, the mechanism remains unclear.

To address these questions, experiments need to develop new high-resolution edge

diagnostic and combine several diagnostics to measure turbulence, density and temperature gradients, and all flow components in the main ion radial force balance equation simultaneously. Finally, the physics described by the simple L-I-H transition model should be captured by suitable fluid or gyrofluid edge-turbulence simulation codes. These could be used to gain deeper insights into the physics before turning to gyrokinetic-based large-scale simulations.

References

[1] Wagner F. *et al* 1982 *Phys. Rev. Lett.* **49** 1408

[2] Shimada M. *et al* 2007 Progress in the ITER Physics Basis, Chapter 1: Overview and summary *Nucl. Fusion* **47** S1

[3] Martin Y.R. *et al* 2008 *J. Phys.: Conf. Ser.* **123** 012033

[4] Wagner F. 2007 *Plasma Phys. Control. Fusion* **49** B1-B33

[5] Terry P.W. 2000 *Rev. Mod. Phys.* **72** 109

[6] Burrell K.H. 1997 *Phys. Plasmas* **4** 1499

[7] Biglari H., Diamond P.H. and Terry P.W. 1990 *Phys. Fluids* **B2** 1

[8] Hahm T.S. and Burrell K.H. 1995 *Phys. Plasmas* **2** 1648

[9] Conner J.W. and Wilson H.R. 2000 *Plasma Phys. Control. Fusion* **42** R1-R74

[10] Zohm H. *et al* 1994 *Phys. Rev. Lett.* **72** 222

[11] Cordey J. *et al* 1995 *Nucl. Fusion* **35** 505

[12] Colchin R.J. *et al* 2002 *Phys. Rev. Lett.* **88** 255002

[13] Colchin R.J. *et al* 2002 *Nucl. Fusion* **42** 1134

[14] Rudakov D.L. *et al* 2001 *Plasma Phys. Controlled Fusion* **43** 559

[15] Kim E.-J. and Diamond P.H. 2003 *Phys. Rev. Lett.* **90** 185006

[16] Itoh S-I *et al* 1991 *Phys. Rev. Lett.* **67** 2485

[17] Diamond P.H. *et al* 1994 *Phys. Rev. Lett.* **72** 2565

[18] Diamond P.H. *et al* 2005 *Plasma Phys. Controlled Fusion* **47** R35

[19] Shaing K.C. and Crume E.C. 1989 *Phys. Rev. Lett.* **63** 2369

[20] Chang C.S., Kue S. and Weitzner H. 2002 *Phys. Plasmas* **9** 3884

[21] Fujisawa A. 2009 *Nucl. Fusion* **49** 013001

[22] Wolfrum E. 2012 *Nucl. Fusion* **54** 124002

[23] Sauter P. *et al* 2012 *Nucl. Fusion* **52** 012001

[24] Ryter F. *et al* 2009 *Nucl. Fusion* **49** 062003

[25] Ryter F. *et al* 2012 *Nucl. Fusion* **52** 114014

[26] Ma Y. *et al* 2012 *Nucl. Fusion* **52** 023010

[27] Meyer H. *et al* 2011 *Nucl. Fusion* **51** 113011

[28] Gohil P. *et al* 2011 *Nucl. Fusion* **51** 103020

[29] Gohil P. *et al* 2010 *Nucl. Fusion* **50** 064011

[30] Gohil P. *et al* 2009 *Nucl. Fusion* **49** 115004

[31] Maingi R. *et al* 2010 *Nucl. Fusion* **50** 064010

[32] Kaye S.M. *et al* 2011 *Nucl. Fusion* **51** 113019

[33] Xu G.S. *et al* 2011 *Nucl. Fusion* **51** 072001

[34] Zweben S. J. *et al* 2007 *Plasma Phys. Control. Fusion* **49** S1

[35] Estrada T. *et al* 2010 *Europhys. Lett.* **92** 35001

[36] Estrada T. *et al* 2011 *Phys. Rev. Lett.* **107** 245004

[37] Conway G.D. *et al* 2011 *Phys. Rev. Lett.* **106** 065001

[38] Schmitz L. *et al* 2012 *Phys. Rev. Lett.* **108** 155002

[39] Zweben S.J. *et al* 2010 *Phys. Plasmas* **17** 102502

[40] Sechrest Y. *et al* 2011 *Phys. Plasmas* **18** 012502

[41] Zweben S.J. *et al* 2012 *Plasma Phys. Controlled Fusion* **54** 025008

[42] McKee G.R. *et al* 2009 *Nucl. Fusion* **49** 115016

[43] Yan Z. *et al* 2011 *Proc. 53rd APS Meeting of Plasma Physics (Salt Lake City, November 14–18, 2011)* GO4.006

[44] Xu G.S. *et al* 2011 *Phys. Rev. Lett.* **107** 125001

[45] Xu M. *et al* 2012 *Phys. Rev. Lett.* **108** 245001

[46] Xu G.S. *et al* 2012 *Phys. Plasmas* **19** 122502

[47] Miki K. *et al* 2012 *Phys. Plasmas* **19** 092306

[48] Manz P. *et al* 2012 *Phys. Plasmas* **19** 072311

[49] Smolyakov A.I. and Diamond P.H. 1999 *Phys. Plasmas* **6** 4410

[50] Gürcan Ö.D. *et al* 2012 *Phys. Rev. Lett.* **109** 155006

[51] Li J. and Wan B. 2011 *Nucl. Fusion* **51** 094007

[52] Liu S.C. *et al* 2012 *Rev. Sci. Instrum.* **83** 123506

[53] Fedorczak N. *et al* 2012 *Phys. Plasmas* **19** 122302

[54] Xu G.S. *et al* 2003 *Phys. Rev. Lett.* **91** 125001

[55] Liu A.D. *et al* 2009 *Phys. Rev. Lett.* **103** 095002

[56] Maqueda R.J. *et al* 2003 *Rev. Sci. Instrum.* **74** 2020

[57] Yan N. *et al* 2011 *Plasma Sci. Technol.* **13** 410

[58] Stotler D. *et al* 2003 *J. Nucl. Mater.* **313-316** 1066

[59] Stotler D. *et al* 2007 *J. Nucl. Mater.* **363-365** 686

[60] Munsat T. and Zweben S.J. 2006 *Rev. Sci. Instrum.* **77** 103501

[61] Terry J. *et al* 2005 *J. Nucl. Mater.* **337-339** 322

[62] McKee G.R. *et al* 2004 *Rev. Sci. Instrum.* **75** 3490

[63] Holland C. *et al* 2004 *Rev. Sci. Instrum.* **75** 4278

[64] Zweben S.J. *et al* 2004 *Nucl. Fusion* **44** 134

[65] Zhang W. *et al* 2010 *Rev. Sci. Instrum.* **81** 113501

[66] Sánchez E. *et al* 2005 *J. Nucl. Mater.* **337–339** 296

[67] Xu G.S. *et al* 2009 *Nucl. Fusion* **49** 092002

[68] Xu G.S. *et al* 2011 *Plasma Sci. Technol.* **13** 397

[69] Wagner F. *et al* 1984 *Phys. Rev. Lett.* **53** 1453

[70] H. Qin *et al* 2000 *Phys. Plasmas* **7** 991

Acknowledgements

This work was supported by the National Magnetic Confinement Fusion Science Program of China under Contracts Nos. 2011GB107001, 2011GB101000, 2010GB104001, 2013GB107003 and 2012GB101000, the National Natural Science Foundation of China under Contracts Nos. 11075181, 11021565, 10990212, 11105177 and the Sino Danish Center for Education and Research.

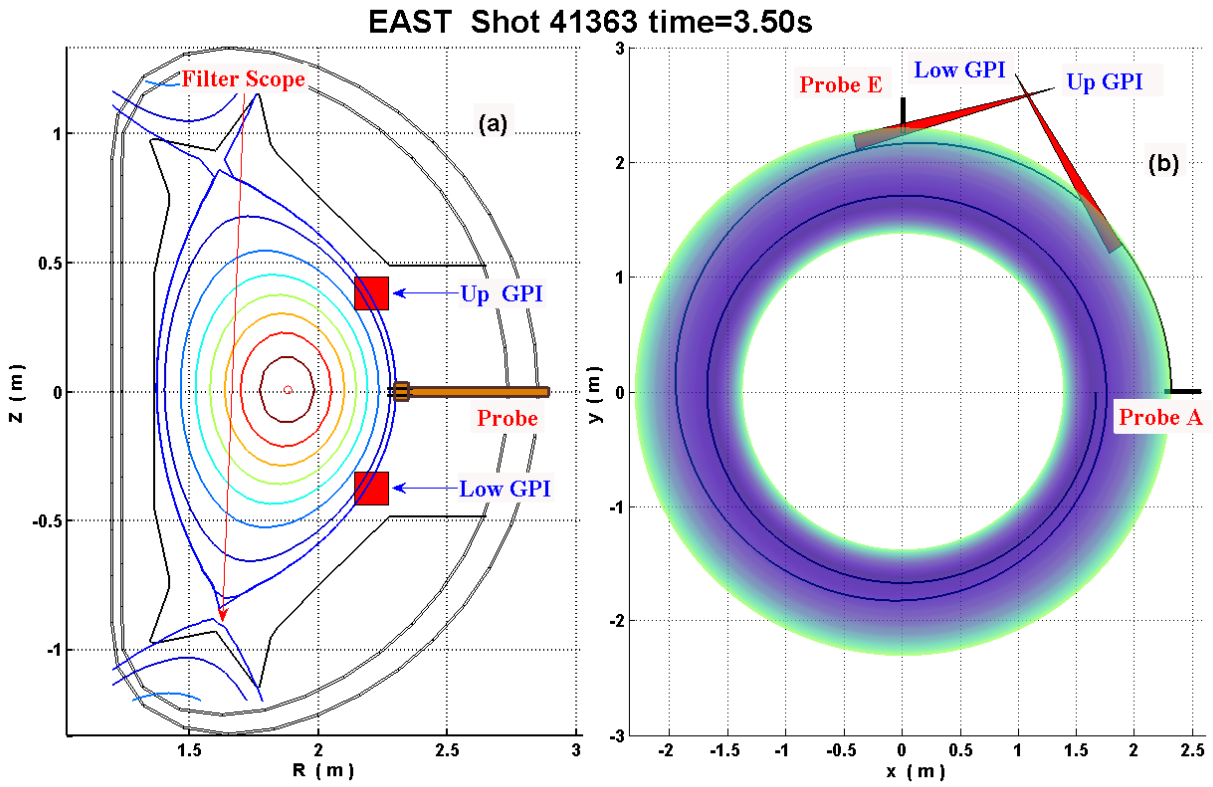

Fig. 1. Illustration of the location of the new dual GPI diagnostic system, along with the two midplane reciprocating probe systems and the sightline of the filter scope system on EAST. (a) Cross-section view of the two imaging objective areas, up-down symmetrical about the midplane, separated poloidally by ~100° around the magnetic axis; (b) Top view of the two GPI sightlines with two gas-cloud objective plane separated toroidally by 66.6°.

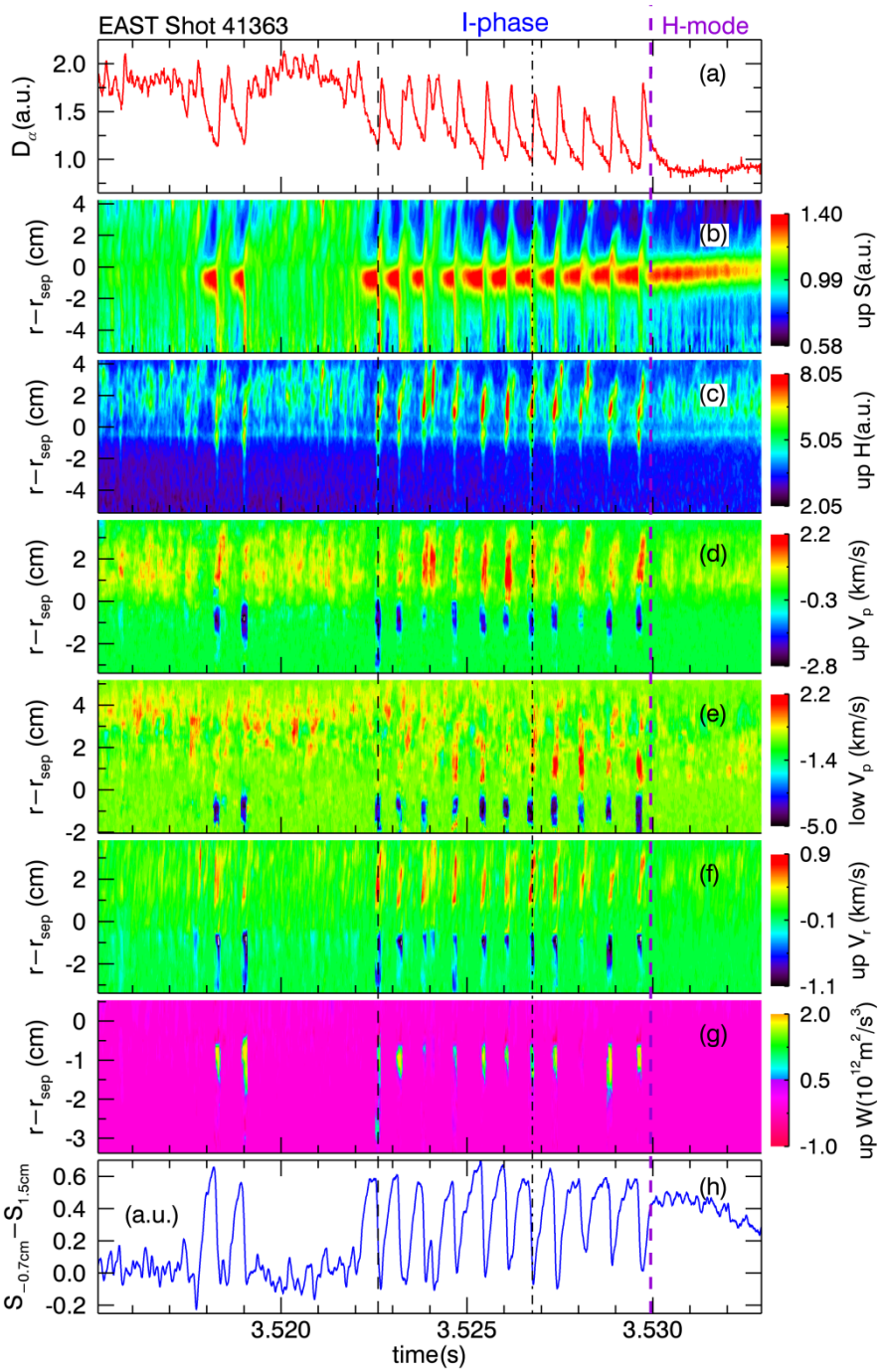

Fig. 2. The time evolution of (a) divertor D_α emission across a dithering L-H transition, the poloidally-averaged radial profiles of (b) relative GPI emission intensity, (c) turbulence fluctuation level, (d) turbulence poloidal velocity from the upper GPI and (e) from the lower GPI, (f) turbulence radial velocity from the upper GPI, and (g) turbulence-driven Reynolds work from the upper GPI at the plasma edge, displayed in a linear false color scale. (h) The difference in the relative GPI emission intensity between two radial locations, i.e., 0.7 cm inside the separatrix and 1.5 cm outside the separatrix.

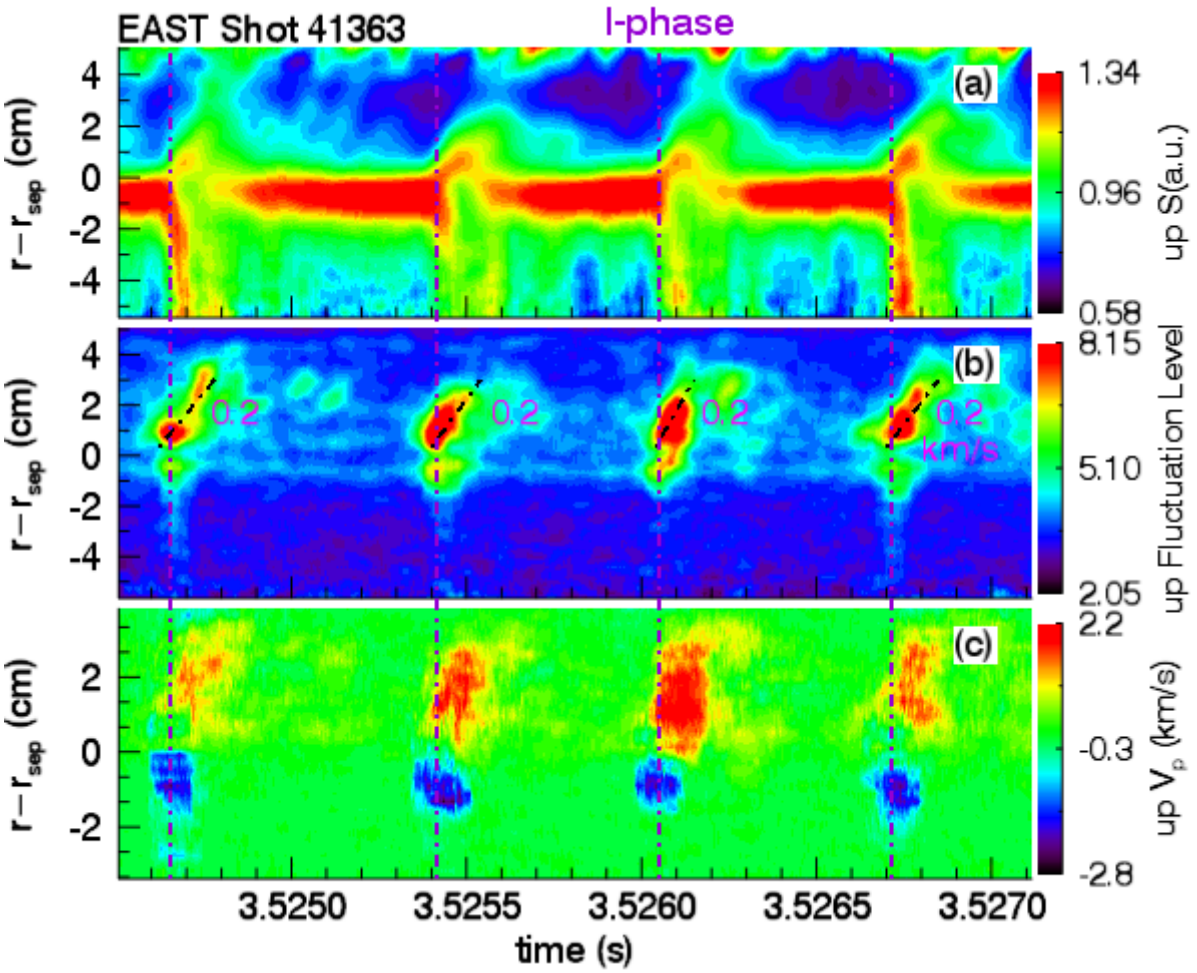

Fig. 3. The partial enlarged details of Figs. 2(b), (c) and (d). The time evolution of the poloidally-averaged radial profiles of (a) relative GPI emission intensity, (b) turbulence fluctuation level, and (c) turbulence poloidal velocity from the upper GPI system at the plasma edge during an I-phase, displayed in a linear false color scale.

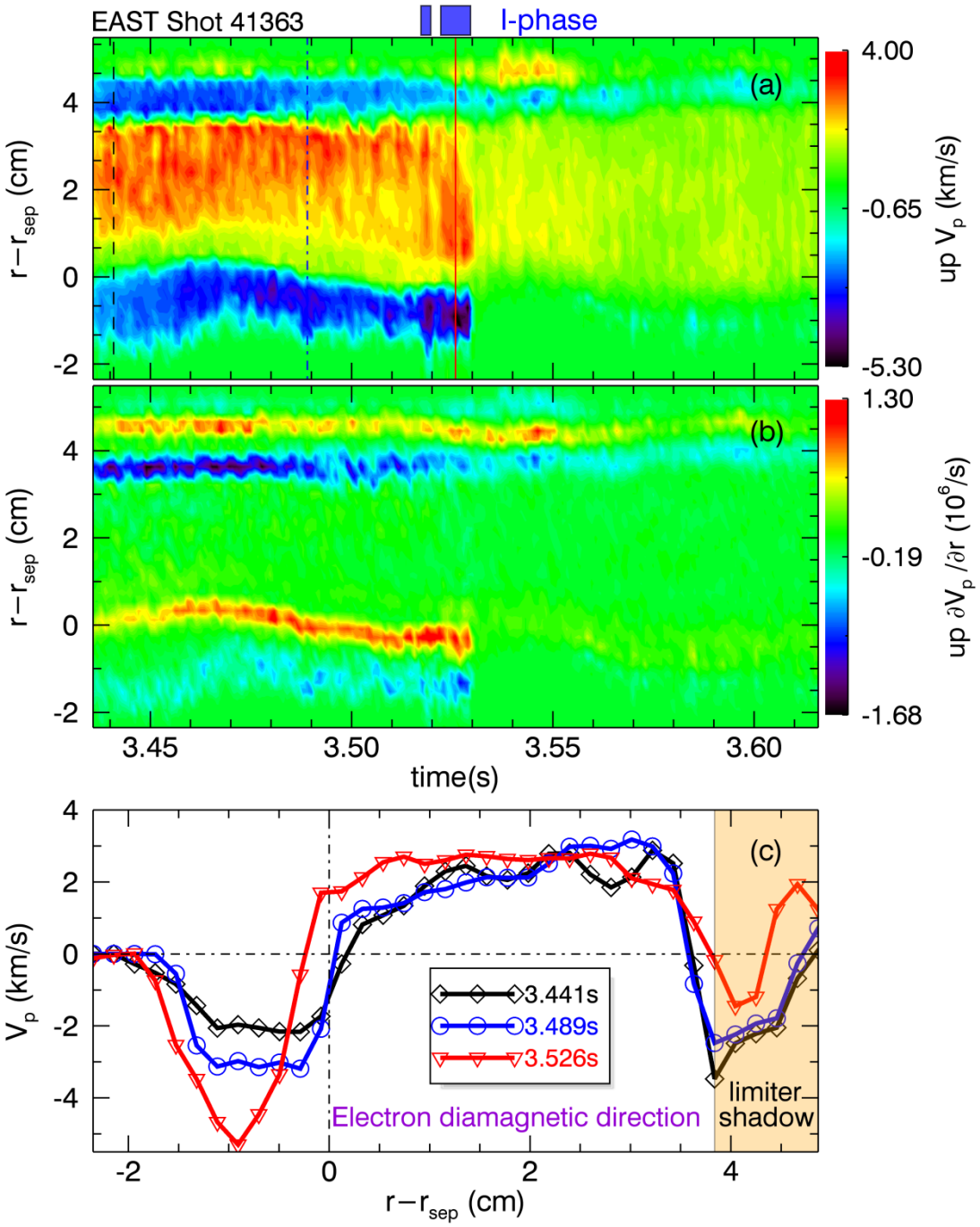

Fig. 4. The time evolution of the poloidally-averaged radial profiles of (a) turbulence poloidal velocity, V_p, and (b) shearing rate of the poloidal velocity, $\partial V_p/\partial r$, from the upper GPI system at the plasma edge across a dithering L-H transition, displayed in a linear false color scale. (c) The radial profiles of poloidal velocity, corresponding to the time slices marked as vertical lines in (a). The blue color bars at the top indicate the time windows for the I-phases shown in Fig. 2.

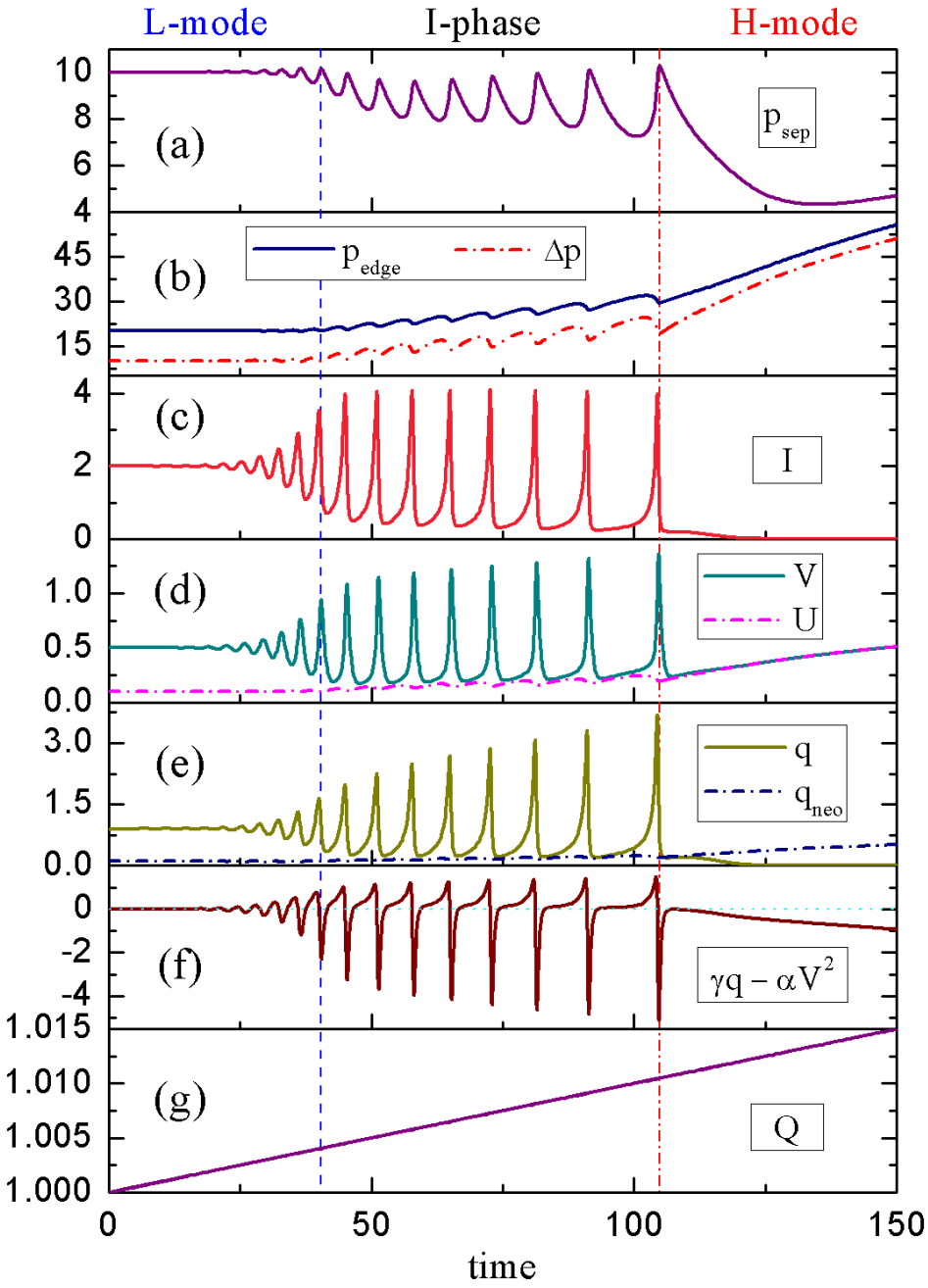

Fig. 5. Modeling of the L-I-H transition with a self-consistent 0D model. The time evolution of (a) pressure at the separatrix, p_{sep}, (b) pressure inside the separatrix, p_{edge}, and edge pressure difference, $\Delta p = p_{edge} - p_{sep}$, (c) turbulence intensity, I, (d) total flow shear, V, and equilibrium flow shear, U, (e) turbulent flux, q, and neoclassical flux, q_{neo}, (f) imbalance between the drive and damping of turbulence, (g) input heating power flux, Q.

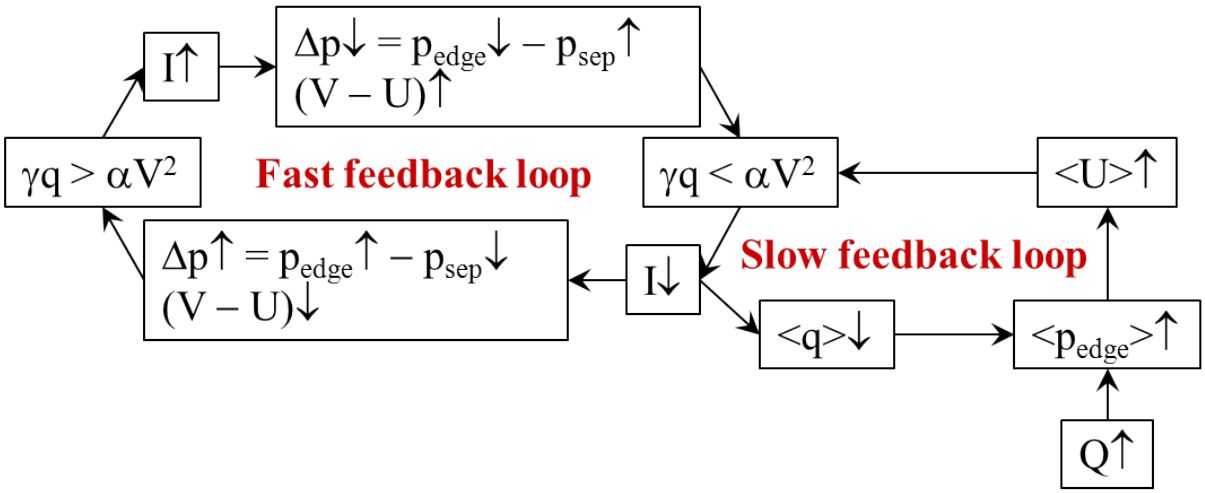

Fig. 6. Schematic block diagram of the two feedback loops in the 0D L-I-H transition model. The fast and slow feedback loop is associated with the zonal flow shear, (V – U), and the equilibrium flow shear, <U>, respectively, where <⋯> denotes the time average over a dithering cycle period.